Chromatographic formation of a triadic band of lithium in hydrated LTA zeolite: an investigation on lithium isotope separation effects by ion exchange

Atsushi Ishikawa*, Mie Sasaki, Susumu Narita, Akari Takeuchi,

Hiroshi Ohki, and Kazuo Yoshino

Department of Chemistry, Faculty of Science, Shinshu University,

Matsumoto 390-8621, Japan

Microporous and Mesoporous Materials

received , 2016

*Corresponding author. fax: +81-263-37-2559.

E-mail address: ishikaw@shinshu-u.ac.jp (A. Ishikawa).

Abstract

Lithium concentrations [Li] and isotopic ratios [^{7}Li]/[^{6}Li] were measured for effluent fractions from a biphasic zeolite column. The biphasic state was ascribed to a mixture of hydrated Linde Type A (LTA) zeolites, $[Li_{0.08}(NH_4)_{0.92}]A$ and $[Li_{0.33}(NH_4)_{0.67}]A$, which were formed by Li ion exchange from hydrated ammonium in the form $(NH_4)_{12}[Al_{12}Si_{12}O_{48}]\cdot nH_2O$ (NH_4A). The biphasic Li band of the column was displaced by ion exchange with a solution of NH_4NO_3. A constant [Li] with a much lower level than the concentration of NH_4^+ in the displacer (NH_4NO_3) was observed for the effluent from a short column. This constant lower level of [Li] was attributable to the biphasic state. On this [Li] plateau of the effluent, the level of [^{7}Li] shifted higher than the original isotopic composition of the Li feed, whereas ^{6}Li was concentrated on the biphasic zeolite solid. The accumulation of ^{6}Li in the zeolite proceeded by a mechanism of differential

elution of ^{7}Li from the biphasic zeolite. For the long column experiment, a significant enrichment of ^{6}Li in the zeolite was observed, whereby a triadic band of Li was probably formed in the column. Two monophasic and a biphasic state were assigned. The biphasic band was deemed to push the monophasic bands forward, thereby enriching the monophasic bands with ^{7}Li, while ^{6}Li accumulated at the end of the biphasic band. The trio structure of the Li band and isotopic discrimination in the band were analyzed.

1. Introduction

The microstructures of solid materials are important in that they can influence certain macroscopic properties. The formation of structures at the nanometer scale that involve phase separation by spinodal decomposition [1–5] can improve material performance and often results in new properties due

to new arrangements of atoms. Typical examples are glasses [6-9], magnets [10-12], alloys [3,13-17], ceramics [18-21], and polymers [22,23]. The nucleation and growth mechanism [6,7] also influences the formation of microstructures.

Recently, a new type of spinodal phase separation induced by ion-exchange was reported [24] for a hydrated Linde Type A (LTA) zeolite. The ammonium form of the hydrated LTA zeolite, $(NH_4)_{12}[Al_{12}Si_{12}O_{48}]\cdot n\ H_2O$ (NH_4A), showed two distinct solid phases, $[Li_{0.08}(NH_4)_{0.92}]A$ and $[Li_{0.33}(NH_4)_{0.67}]A$ hydrates, by Li ion exchange with aqueous solutions at 295 K. The excess Gibbs function determined from ion-exchange-isotherm measurements indicated spinodal and binodal phase separation. Powder X-ray diffraction analysis confirmed this phase separation. (The diffraction peaks and the lattice constants of hydrated $[Li_x(NH_4)_{1-x}]A$ were reported in the reference [24].)

The biphasic zeolite has a unique property [24, 25]. When the biphasic zeolite was formed by Li ion exchange, ^7Li isotopes

moved to the aqueous phase as tetrahydrate $[Li(OH_2)_4]^+$, whereas ^6Li isotopes were left in the six-membered oxygen rings of the biphasic zeolite with two hydrated water molecules of the $[Li_{0.08}(NH_4)_{0.92}]A$ and $[Li_{0.33}(NH_4)_{0.67}]A$ hydrates. In aqueous solution, strong hydration action captures ^7Li isotopes at the lower levels of the vibrational energy of ^7Li tetrahydrates. At the same time, ^6Li isotopes are left in the low-frequency vibrational levels at the center of the six-membered oxygen rings with two water of hydration molecules. These molecular vibration levels were clarified in *ab initio* molecular orbital calculations [25].

A single-stage separation factor, expressed as $\alpha = ([^7Li]/[^6Li])_{aq}/([^7Li]/[^6Li])_{solid}$, was measured as a function of the Li molar fraction (Li_x) of the zeolite, and had a value of $\alpha = 1.02$ for $0.0 < Li_x < 0.33$, while for a higher filling range of $0.33 < Li_x < 1.0$, the value decreased to $\alpha = 1.01$. The constant α value ($\alpha = 1.02$) over a wide range ($0.08 < Li_x < 0.33$) was

attributable to the coexistence of two equilibria in aqueous solution: $NH_4A + Li^+_{aq} \leftrightarrow [Li_{0.08}(NH_4)_{0.92}]A + NH_4^+{}_{aq}$, and $NH_4A + Li^+_{aq} \leftrightarrow [Li_{0.33}(NH_4)_{0.67}]A + NH_4^+{}_{aq}$. $\alpha = 1.02$ was also observed for a lower loading state ($Li_x < 0.08$) [24].

The constant α of 1.02 over a wide range of low filling values ($Li_x < 0.33$) was evident from column experiments [25]. When an NH_4A column was fed with a $LiNO_3$ solution ([Li] = 50 mM) at 293 K, the Li concentration ([Li]) of the effluent fractions showed a plateau ([Li] = 20 mM) with a ^7Li separation effect. The biphasic state of the zeolite restricted [Li] to a constant value of [Li] = 20 mM, which corresponds to the plateau of the isotherm for the forward ion exchange, $NH_4A + Li^+ \rightarrow [Li_x(NH_4)_{1-x}]A + NH_4^+$.

The biphasic state is deemed essential to accumulate ^6Li in the zeolite, and is effective for continuous release of ^7Li isotopes. Therefore in this investigation, column experiments were conducted while maintaining the biphasic state of the

zeolite. The lithium concentrations [Li] and isotopic ratio [^{7}Li]/[^{6}Li] were measured for the effluent fractions from the biphasic zeolite columns. The mechanism for the accumulation of ^{6}Li in a column was studied. Furthermore, a long-column experiment was carried out to clarify the effect of the development of the biphasic band. As a new aspect of the ion-exchange-science of zeolites, the structure of the Li band and the discrimination of Li isotopes based on the phase separation phenomenon are discussed.

2. Experimental

All chemicals used in the experiments were reagent grade. The ammonium form of LTA zeolite (NH_4A) was prepared from commercial NaA powder (Tosoh) by ion exchange [25].

The ion-exchange solution was NH_4NO_3 with pH 8, which was prepared by mixing an acid (HNO_3) and a base (NH_3) to obtain

the desired pH. The commercial solid NH_4NO_3 regent contained considerable amounts of Na as an impurity; therefore, NH_4NO_3 solution prepared from the acid and base had very low impurity levels of sodium. The prepared NH_4NO_3 solution thus completely exchanged the Na ions in the zeolite.

Following the removal of the smaller particles less than ca. 1 μm by decantation, the resulting homogeneous powder of NH_4A (ca. 10 μm) was packed into a glass tube column (1 cm internal diameter). The size of the particles was confirmed using a conventional optical microscope (Nikon) with a hemocytometer (Thoma cell counting chamber).

Lithium nitrate solution at pH 8 was prepared by mixing LiOH and HNO_3, and was fed into the NH_4A column to form a broad adsorption band of $[Li_x(NH_4)_{1-x}]A$ throughout the column. Ammonium nitrate solution at pH 8 was used for the elution of Li from the column.

The feeds and the eluents were run with a pressure device

operated at constant pressure below 1 kg/cm^2. The flow rate and the temperature were maintained at 5 cm^3 h^{-1} and 288 K, respectively. The effluent fractions were collected hourly. The column experiments were performed for different column lengths (Table 1). For a long column (60 cm), three short columns were connected with fine tubes.

The feed and eluent concentrations were almost the same, and the feed volume was nearly constant. The experimental conditions are summarized in Table 1.

A flame-emission spectrometer (Shimadzu AA650) was used for [Li] measurements of the feed and effluent. The ammonium ion concentration was measured with an ammonium electrode (TOA Electronics Ltd. IM-55G). When the molar fraction of NH_4NO_3 in the effluents exceeded 0.25, the emission intensity for Li atoms increased up to 110%. For this reason, the measured [Li] values in the effluent fractions were corrected using the conservation principle, where the total amount of lithium in the effluent

equals that in the feed (Table 2). The total amount of Li of the effluent was calculated by numerical integration with a software of mathematics [26].

A thermal ionization mass spectrometer (Finnigan MAT 262) was operated using the double filament (Re-Ta) technique for the isotopic measurements of $[^{7}Li]/[^{6}Li]$. In the present analysis, the accuracy of the isotopic measurements was improved by the addition of a small amount of $La(NO_3)_3$ to the $LiNO_3$ samples. A drop of the sample $LiNO_3$ solution (0.5 μL) containing $La(NO_3)_3$ on a tantalum filament was evaporated at 0.6 A and finally dehydrated within 30 s at 2.0 A. The temperature of the sample was 393±10 K, and was monitored with a radiothermometer (Minolta TA0510bF). The formation of lanthanum oxide on the surface protected the hygroscopic $LiNO_3$ sample from water in the ambient air (When a $LiNO_3$ sample contains a small amount of water, the intensity of the Li isotope beams are unstable). Stable intensities of the Li isotope beams

generated from the $LiNO_3$ sample on the Ta filament were achieved by heating the ionization filament (Re) of the mass spectrometer ion source. The signal intensity of the ^7Li and that of ^6Li were alternately acquired with the Faraday cup of the mass spectrometer by switching the magnetic field strength. After the repeated measurements, the average isotopic ratio for the original $LiNO_3$ feed solution for 21 samples was R_{feed} = 12.51±0.02 (95% confidence limits).

3. Results

The measured C_{ef} = [Li] and R_{ef}= [^7Li]/[^6Li] for the effluent fractions from the experiments (Table 1) are shown in Figs. 1 and 2. All the effluent data were interpolated and the amounts of both isotopes of Li in the total effluent were calculated (Table 2) with the software of mathematics [26]. The calculated isotopic ratios for the total effluent (R_0 = 12.5) of Entries

1-4 were equal to each other and were consistent with the original value of the feed (R_{feed} = 12.51). The R_{ef} and C_{ef} values are plotted as R_{ef}/R_0, and C_{ef}/C_0, respectively, where C_0 represents the $LiNO_3$ concentration in the feed, and also indicates the NH_4NO_3 concentration as eluent (Table 1). The origin of the abscissa in both figures indicates the switchover from Li feed to Li elution.

While feeding the $LiNO_3$ solution (C_0 = ca. 50 mM), the effluent concentration [Li] = C_{ef} immediately reached a plateau (C_{ef} = 20 mM) for Entries 1-3 (Fig. 1), which corresponds to C_{ef}/C_0 = 0.4. After switching from feeding to elution with NH_4NO_3 (C_0 = ca. 50 mM), the plateau ([Li] = 20 mM) maintained an unsaturated value of C_{ef}/C_0 = 0.4. The isotopic ratios were stable at R_{ef} = 12.7 over a wide range of elution, which was higher than the original value (R_0 = 12.5, Table 2) and corresponded to R_{ef}/R_0 = 1.02.

Figure 2 shows plots of C_{ef}/C_0 and R_{ef}/R_0 for Entry 4. The

effluent data for Entry 1 are also displayed for comparison. In the feeding process for Entry 4, all the Li ions in the feed were absorbed into the zeolite column. After the beginning of Li elution, the Li concentration slowly increased (up to C_{ef} = 20 mM) until the plateau (C_{ef}/C_0 = 0.4), which appeared in the latter half of the elution volume (500–750 mL). In the last elution of Li, significant ^{6}Li enrichment (R_{ef} = 7.5) was obtained (R_{ef}/R_0 = 0.6 at V = 750 mL). Over almost the entire range of the elution volume, the observed Li isotopic ratios for Entry 4 were higher those for Entry 1. The isotopic ratio R_{ef}/R_0 = 1.04 was high and almost constant over a wide range of effluent volume (200–500 mL).

4. Discussion

4.1. Displacement Chromatography

In ion exchange chromatography, the separation of ions is accomplished in one of two ways: by the development of ion elution or ion displacement [27]. In Figure 1, the wide rectangular effluent curves of Li (Entries 1 to 3) are typical of displacement chromatography. In the displacement of the ion absorption bands of the column, the effluent concentration for the plateau is typically the same level as the displacer (C_{ef}/C_0 = 1.0). However, for every experiment in this study, the effluent plateau was suppressed (C_{ef}/C_0 = 0.4), presumably by the formation of biphasic zeolite. (The two phases were reported [24, 25] as $[Li_{0.08}(NH_4)_{0.92}]A$ and $[Li_{0.33}(NH_4)_{0.67}]A$.)

The lithium ions were distributed between the solid and the solution according to the equilibrium condition C_{ef}/C_0 = 0.4 with the isotope effect. (In the case of the equilibrium condition C_{ef}/C_0 = 1.0, no isotope effect is observed in the effluent, because every lithium ion in the feed simply moves to the effluent via a column solid.) The concentrations of both

isotopes in the effluent were analyzed in the following way.

The effluent concentration C_{ef} = [Li] is expressed as a function of the effluent volume V using the following empirical equation in this study.

$$[\mathrm{Li}] = C_{ef} = \frac{C_{max}}{2}\left[1 + \tanh\left(\frac{V - V_f}{V_{g\text{-}f}}\right)\tanh\left(\frac{V_r - V}{V_{g\text{-}r}}\right)\right], \quad (1)$$

Here, C_{max}, V_f, V_r, V_{g-f}, and V_{g-r} are the height of the plateau, the frontal volume, the rear volume, the gradient factor for the front, and the gradient factor for the rear, respectively. The pair of hyperbolic functions expresses the rectangular shape of the effluent concentration. The function y = tanh x is step-like from y = -1 to y = 1 at x = 0, so the function y = tanh $(x-x_f)$ tanh $(-x+x_r)$ is rectangular in the region $\{x_f < x < x_r, -1 < y < 1\}$, when x_r is sufficiently far from x_f. Separate experiments conducted using ion-exchange resin confirmed that Eq. (1) holds for any effluent curve, including an elution

development curve. The function tanh $(x-x_f)$ tanh $(-x+x_r)$ exhibits a peak when x_r is close to x_f.

In Fig. 3, the development of Li band displacement ($[^7Li + ^6Li]$) for Entry 1 is shown with the curve of Eq. (1) determined by FindFit package of the software [26]. The effluent concentrations of both isotopes, $[^7Li] = [Li]\,R_{ef}/(1+R_{ef})$ and $[^6Li] = [Li]/(1+R_{ef})$, are depicted using the polynomial $R_{ef} = \sum_{n=1}^{7} a_n V^n$ calculated with Fit command of the software [26].

The curve for $[^6Li]$ multiplied by $R_0 = 12.5$ was also added. The isotopic composition in the feed is expressed as $[^7Li]/[^6Li] = R_0 = 12.5$; therefore, the difference between $12.5[^6Li]$ and $[^7Li]$ indicates isotopic deviation from the original ($12.5[^6Li] = [^7Li]$) ratio.

The curve of $12.5[^6Li]$ has a peak just before the end of effluent elution. At the same time, based on the conservation principle ($[Li] = [^7Li + ^6Li] = \text{constant}$), a corresponding deficit of $[^7Li]$ is observed, although it is not obvious at the

scale of Fig. 3.

The elution level of [^{7}Li] shifted the 12.5[^{6}Li] level upward over a wide range of effluent volume. This continuous isotope effect is the main mechanism for [^{6}Li] accumulation, which emerges as a peak just before the end of the chromatographic elution.

4.2. Isotopic enrichment in the biphasic zeolite after the elution process

For Entry 1 (Table 1), the amounts of each Li isotope, which left in the zeolite from the effluent, were calculated from the fitting functions of the effluent (Fig.3). The results are shown in Fig. 4. Lithium ions were captured in the zeolite in the feeding process (V = -240 to V = 0 mL) and were released from the zeolite at a constant rate in the elution process (V = 0 to 420 mL). The Li isotopic ratio for the zeolite ($R_{zeolite}$) was

almost equal to that for the feed solution in the feeding process, while it was gradually decreased in the elution process. Significant enrichment of ^{6}Li occurred at the last stage of elution, where $R_{zeolite}/R_0$ = 0.77 at V = 430 mL. Further enrichment was observed for Entry 4 (Fig. 5) with $R_{zeolite}/R_0$ = 0.6 at V = 750 mL, because the higher isotopic shifts of R_{ef}/R_0 = 1.04 were effective over a wide range of effluent volume (Fig. 2).

4.3. Mechanism for ^{6}Li enrichment in the zeolite

The separation factor α, for the Li isotopes is defined as:

$$\alpha = \frac{[^{7}\mathrm{Li}] / [^{6}\mathrm{Li}]}{[\overline{^{7}\mathrm{Li}}] / [\overline{^{6}\mathrm{Li}}]} = \frac{[^{7}\mathrm{Li}][\overline{^{6}\mathrm{Li}}]}{[\overline{^{7}\mathrm{Li}}][^{6}\mathrm{Li}]} = \frac{\eta(1-\xi)}{\xi(1-\eta)}, \qquad (2)$$

where concentrations with a bar represent the solid phase and those without a bar represent the liquid phase. The parameter ξ is the molar fraction of ^{7}Li in the solid. Similarly, the

parameter η represents the molar fraction of ^{7}Li in aqueous solution. η and ξ are related through the isotopic separation factor, α:

$$\eta = \frac{\alpha\xi}{1+(\alpha-1)\xi}. \qquad (3)$$

There is initially a certain amount (m) of Li in the zeolite solid. If a small amount (Δm) of Li in the solid moves to the aqueous phase, then the amount of Li in the solid decreases to $m-\Delta m$, and the molar fraction of ^{7}Li in the solid also decreases to $\xi-\Delta\xi$ due to the isotopic effect, whereas the amount of ^{7}Li ($\eta\Delta m$) in the aqueous solution increases. The balance of ^{7}Li between the solid and liquid phases is expressed as:

$$\xi m = (m-\Delta m)(\xi-\Delta\xi)+\eta\Delta m. \qquad (4)$$

In this case, the differential relation is expressed as:

$$\frac{dm}{m} = \frac{d\xi}{\eta - \xi} = \frac{1}{\alpha - 1}\left(\frac{1}{\xi} + \alpha\frac{1}{1-\xi}\right)d\xi. \qquad (5)$$

Integration from the initial amount of Li in the solid (m_0) to an amount m gives:

$$\int_{m_0}^{m}\frac{dm}{m} = \int_{x_0}^{x}\frac{d\xi}{\eta - \xi} = \frac{1}{\alpha - 1}\left(\ln\frac{\xi}{\xi_0} - \alpha\ln\frac{1-\xi}{1-\xi_0}\right) = \ln\frac{m}{m_0}. \qquad (6)$$

Therefore, the separation factor yields:

$$\alpha = \frac{\ln\dfrac{\xi m}{\xi_0 m_0}}{\ln\dfrac{(1-\xi)m}{(1-\xi_0)m_0}} = \frac{\ln\dfrac{m_{Li-7}}{m_{Li-7}(initial)}}{\ln\dfrac{m_{Li-6}}{m_{Li-6}(initial)}}. \qquad (7)$$

This differential elution mechanism is equivalent to the Rayleigh distillation [28], or the differential distillation mechanism [29].

For Entries 1 and 4, the fractional amount of ^{7}Li in the

zeolite is plotted against that of ^{6}Li on a logarithmic scale in Fig. 6. Almost linear relationships were observed for both Entries 1 and 4, which suggests that the differential elution mechanism is generally appropriate. The isotopic separation factors for Entries 1 and 4 were calculated using Eq. (7), and the results are shown in Figure 7. For Entry 4, the calculated α values were high at the initial and final stages of elution, which is attributable to the chromatographic multi-stage separation. The lowest α values were $\alpha = 1.02$ and $\alpha = 1.05$ for Entries 1 and Entry 4, respectively. These are consistent with the continuous isotope effect of the effluent for Entries 1 (R_{ef}/R_0 = 1.02) and 4 (R_{ef}/R_0 = 1.04).

4.4 Formation of the triadic band for Li

Fitting calculations by the software [26] showed that the shape of the effluent curve for Entry 4 was not consistent with

one or two component curves. The effluent curve could be fitted with three components, as expressed by:

$$[\mathrm{Li}] = \sum_{i=1}^{3} C_i = \sum_{i=1}^{3} A_i \left[1 + \tanh\left(\frac{V - V_{f\text{-}i}}{V_{g\text{-}f\text{-}i}}\right)\tanh\left(\frac{V_{r\text{-}i} - V}{V_{g\text{-}r\text{-}i}}\right)\right]. \quad (8)$$

The resultant curves at FindFit command [26] are shown in Fig. 8. (Separate column experiments were conducted, which confirmed monadic, dyadic and triadic bands with an increase in the amount of Li loading on hydrated NH_4A.) The C_3 curve expresses the biphasic band, while the C_2 and C_1 curves correspond to distinct monophasic bands. The two monophasic bands were separated in front of the biphasic band by ion-exchange displacement in the long column. On the other side, the formation of a trio of Li bands is an unexpected phenomenon. When there are three bands in a cation-exchange-resin column, each band typically corresponds to a different chemical element. Therefore, the C_1, C_2, and C_3 curves were regarded as different kinds of ions,

labeled in Fig. 8 as Li-A, Li-B, Li-C, respectively. Each Li-band may be classified as a type of Li occupancy in the zeolite, in accordance with the thermodynamic study [24] of phase separation (Fig. 9). In Figure 9, Li-A is the monophasic Li formed with the lowest occupancy of x in the hydrated zeolite (NH_4A < $[Li_x(NH_4)_{1-x}]A$ < $[Li_{0.08}(NH_4)_{0.92}]A$); Li-B is another monophasic Li formed with an occupancy of x between the binodal and the spinodal ($[Li_{0.08}(NH_4)_{0.92}]A$ < $[Li_x(NH_4)_{1-x}]A$ < $[Li_{0.12}(NH_4)_{0.88}]A$); and Li-C is the biphasic Li within the spinodal curve ($[Li_{0.12}(NH_4)_{0.88}]A$ < $[Li_x(NH_4)_{1-x}]A$ < $[Li_{0.24}(NH_4)_{0.76}]A$).

When the Li-C band displaces the Li-A and Li-B bands forward by ion-exchange, ^7Li isotopes tend to shift ahead toward the former bands, whereas ^6Li isotopes remain in the Li-C band. Finally, at the end of elution, ^6Li accumulation appears as a high peak (Figs. 10 and 11).

5. Conclusion

The chromatographic displacement of the biphasic Li band carries the advantage that ^{6}Li isotopes effectively concentrate in the last effluent. In particular, for the long column, the spinodal decomposition band of Li functions as a displacer band, which displaces ^{7}Li toward the former dyadic band. As a result, ^{6}Li is remarkably left at the end of the band. The formation of the triadic band with isotope separation is a new phenomenon in the field of ion exchange.

Acknowledgments

The authors are grateful to Prof. A. Sasane for encouragement. The ion-exchange experiments were performed on the basis of preliminary experiments conducted by Mr. K. Masago and Mr. H. Nakano. This investigation was supported in part by a Kakenhi Grant-in-Aid (No. 22656211) from the Japan Society for the Promotion of Science (JSPS).

References

[1] E. P. Favvas and A. Ch. Mitropoulos, J. Eng. Sci. Technol. Rev. 1 (2008) 25, and references cited therein.

[2] J. W. Cahn, J. Chem. Phys. 42 (1965) 93.

[3] J. W. Cahn, Trans. Metall. Soc. AIME 242 (1967) 166.

[4] R. W. Haskell, J. Amer. Ceramic Soc. 56 (1973) 355.

[5] J. Goldsbrough, Sci. Prog., Oxf. 60 (1972) 281, and references cited therein.

[6] W. Haller, J. Chem. Phys. 42 (1965) 686.

[7] J. J. Hammel, J. Chem. Phys. 46 (1967) 2234.

[8] R. H. Doremus and A. M. Turkalo, Science 164 (1969) 418.

[9] D. Enke, F. Janowski, W. Schwieger, Microporous Mesoporous Mater. 60 (2003) 19.

[10] B. Ditchek and L. H. Schwartz, Ann. Rev. Mater. Sci. 9 (1979) 219.

[11] K. J. Strnat, IEEE Trans. Magnetics, MAG-6 (1970) 182.

[12] J. Fidler, in G. C. Hadjipanayis (Ed.), Magnetic Hysteresis in Novel Magnetic Materials, Kluwer Academic Publishers, 1997, p. 567.

[13] Y. Murakami, Mater. Sci. Technol. 8 (1996) 213.

[14] A. Guinier, Nature 142 (1938) 569.

[15] G. D. Preston, Proc. Roy. Soc. (London), Ser. A, 167 (1938) 526.

[16] Yu. D. Tiapkin, Ann. Rev. Mater. Sci. 7 (1977) 209.

[17] L. H. Schwartz, NATO ASI Series E, Applied Sciences 83 (1984) 411.

[18] R. C. Garvie, R. H. Hannink, and R. T. Pascoe, Nature 258 (1975) 703.

[19] T. Sakuma, Y. Yoshizawa, and H. Suto, J. Mater. Sci. 21 (1986) 1436.

[20] M. Hillert and T. Sakuma, Acta Metall. Mater. 39 (1991) 1111.

[21] S. R. S. Badwal, Solid State Ionics 52 (1992) 23.

[22] T. Inoue, Prog. Polym. Sci. 20 (1995) 119.

[23] T. D. Ignatova, L. F. Kosyanchuk, T. T. Todosiychuk and A. E. Neterov, Composite Interfaces 18 (2011) 185.

[24] A. Ishikawa, Y. Sakurazawa, J. Shindo, M. Shimada, T. Ishimaru, S. Ishikawa, and A. Sasane, Microporous Mesoporous Mater. 78 (2005) 169.

[25] A. Ishikawa, Y. Mizusawa, S. Ishikawa, A. Sasane, and Y. Mori, Phys. Chem. Chem. Phys. 5 (2003).

[26] S. Wolfram, Mathematica: A System for Doing Mathematics by Computer, Second Edition, Addison-Wesley Publishing Company, Redwood City, California, 1991, and the online Wolfram Mathematica Documentation Center.

[27] F. Helfferich, Ion Exchange, McGraw-Hill, New York, 1962, repr., Dover, New York, 1995, pp. 436-440.

[28] J. W. S. Rayleigh, Phil. Mag. and J. Sci., Series 6, 4 (1902) 521.

[29] J. D. Seader and E. J. Henley, Separation Process

Principles, John Wiley & Sons, Inc., New York, 1998, pp. 681-682.

Table 1

Experimental conditions

Entry	Column length	Feed	Feed volume	Eluent
	L (cm)	C_0 = [Li] (mM)	V_{feed} (mL)	C_0 = [NH_4] (mM)
1	10	50.7	241.0	53.9
2	20	50.4	261.4	49.4
3	30	50.4	241.8	49.4
4	60	53.3	243.2	53.9

Table 2

Amount of Li isotopes in the total effluent fractions

Entry	Li_{feed} (mmol)	$Li_{t\text{-}ef}$ (mmol)	$^{7}Li_{t\text{-}ef}$ (mmol)	$^{6}Li_{t\text{-}ef}$ (mmol)	$R_0 = {}^{7}Li_{t\text{-}ef} / {}^{6}Li_{t\text{-}ef}$
1	12.2	12.2	11.3	0.903	12.5
2	13.2	13.2	12.2	0.979	12.5
3	12.2	12.2	11.3	0.901	12.5
4	13.0	13.0	12.0	0.963	12.5

The suffix t-ef used here is an abbreviation for the total effluent fractions.

Figure Captions

Fig. 1. Column-experiments for Entries 1 to 3 (Table 1): Li concentrations and isotope ratios are indicated with filled and open circles (Entry 1), gray and open squares (Entry 2), and gray and open diamonds (Entry 3), respectively. The horizontal line ($R_{ef}/R_0 = 1$) indicates the origin of the Li-isotope-ratio of the feed solution ($R_0 = 12.5$). The vertical line shows the switching point from Li supply to Li elution.

Fig. 2. Comparison between Entries 1 and 4 (Table 1): Li concentration and isotopic ratios are indicated with filled and open squares (Entry 1), and filled and open circles (Entry 4), respectively. The horizontal line ($R_{ef}/R_0 = 1$) indicates the origin of the feed solution ($R_0 = 12.5$). The vertical line shows the switching point.

Fig. 3. Development of the displacement of the Li band for Entry 1: $[^7Li + ^6Li] = 10.67[1 + \tanh(0.0518(V + 165))\tanh(0.0633(407 - V))]$. The broken lines indicate the effluents of each Li isotope using the expressions in the text with the polynomial, $R_{ef} = [^7Li]/[^6Li] = 12.76 + (1.469\times10^{-3})V - (8.755\times10^{-6})v^2 - (7.710\times10^{-8})v^3 + (5.191\times10^{-10})V^4 - (5.589\times10^{-13})V^5 - (9.678\times10^{-16})V^6 + (1.116\times10^{-19})V^7$. The dotted line shows the magnification of $[^6Li]$ by $R_0 = 12.5$ for comparison with $[^7Li]$ (see the main text).

Fig. 4. Accumulation and subsequent elution of Li (Entry 1). The thin solid line is the amount of both Li isotopes ($^6Li + ^7Li$). The peak indicates the switching from accumulation to elution. The amounts of Li isotopes are shown with broken lines. For comparison between the amount of ^7Li and ^6Li, the amount of ^6Li is magnified by $R_0 = 12.5$ (dotted line). The Li isotope

ratios of the zeolite ($R_{zeolite}/R_0$) are also shown (thick solid line).

Fig. 5. Elution of Li (Entry 4): The amount of ^{6}Li, magnified by R_0 = 12.5 (dotted line) is higher than the elution of ^{7}Li (broken line). Lithium isotope ratios of the zeolite are shown as a thick solid line.

Fig. 6. Mechanism for the differential elution of Li isotopes: The solid line with filled circles is for Entry 1 and the dotted line with open circles is for Entry 4.

Fig. 7. Lithium isotope separation factor (α) for the elution process as a function of the fractional amount of ^{6}Li in the zeolite. The filled circles are for Entry 1 and the open circles are for Entry 4.

Fig. 8. The triadic band of Li appeared in the Entry 4 experiment. Li-A: $C_1 = 4.14(1 + \tanh[0.101(V - 28.3)]\tanh[0.0265(132 - V)])$; Li-B: $C_2 = 8.48(1 + \tanh[0.182(V - 124)]\tanh[0.0152(357 - V)])$; Li-C: $C_3 = 10.25(1 + \tanh[0.0133(V - 356)]\tanh[0.412(757 - V)])$. The measured [Li] (filled circles) and fitted curve (thin solid line) with $[Li] = C_1 + C_2 + C_3$ are also shown.

Fig. 9. The phase separation diagram of hydrated $[Li_x(NH_4)_{1-x}]A$ cited from the reference [24]. The calculated spinodal (convex solid line) and binodal (dotted line) curves for the molar fractions of Li in the zeolite (x) are shown. The critical temperature is $T_c = 405$ K. The calculated ion-exchange isotherm of 295 K (sigmoidal solid line) is also plotted. The Li molar fractions of the aqueous solution are denoted by y. Closed and open circles indicate forward ($Li^+ + NH_4A \rightarrow [Li_x(NH_4)_{1-x}]A + NH_4^+$)

and reverse ($LiA + NH_4^+ \rightarrow Li^+ + [Li_x(NH_4)_{1-x}]A$) ion-exchange data, respectively. The sinusoidal behavior of the isotherm ($0.12 < x < 0.24$) implies the phase separation of the hydrated state zeolite. The thermodynamic calculations of the diagram from the ion-exchange data are described in the original [24].

Fig. 10. ^6Li enrichment and ^7Li depletion at the end of the effluent (Entry 4). The broken lines indicate the effluents of the Li isotopes using the expression in the text with the polynomial: $R_{ef} = [^7Li]/[^6Li] = 17.10 - (1.297\times10^{-1})V + (1.629\times10^{-3})v^2 - (1.025\times10^{-5})v^3 + (3.487\times10^{-8})V^4 - (6.493\times10^{-11})V^5 + (6.214\times10^{-14})V^6 - (2.386\times10^{-17})V^7$. The dotted line shows the magnification for $[^6Li]$.

Fig. 11. Lithium isotope concentrations for the Li-A, Li-B, and Li-C bands (solid lines). The dotted line indicates the

magnification for [^{6}Li].

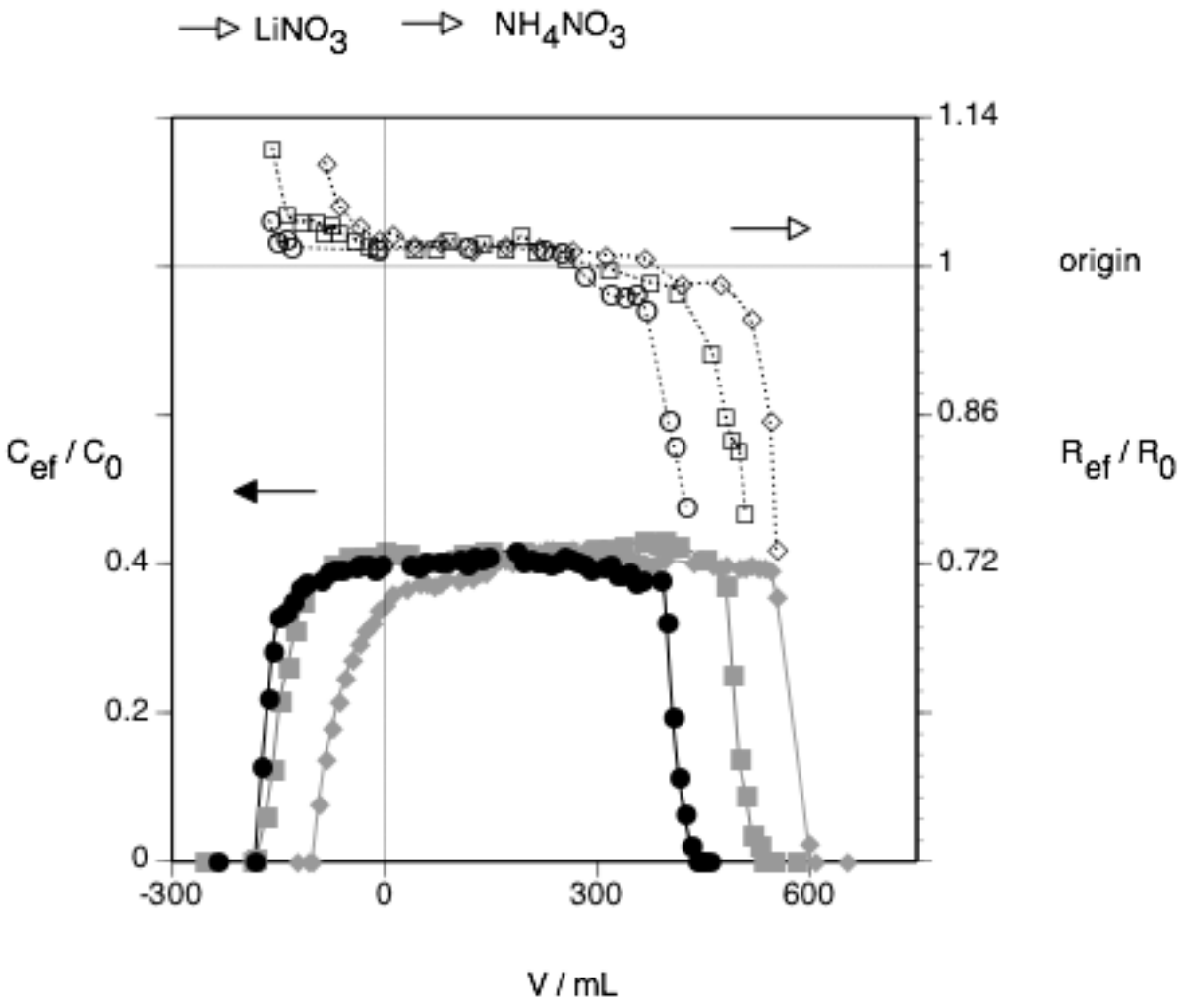

Fig. 1, A. Ishikawa et al.

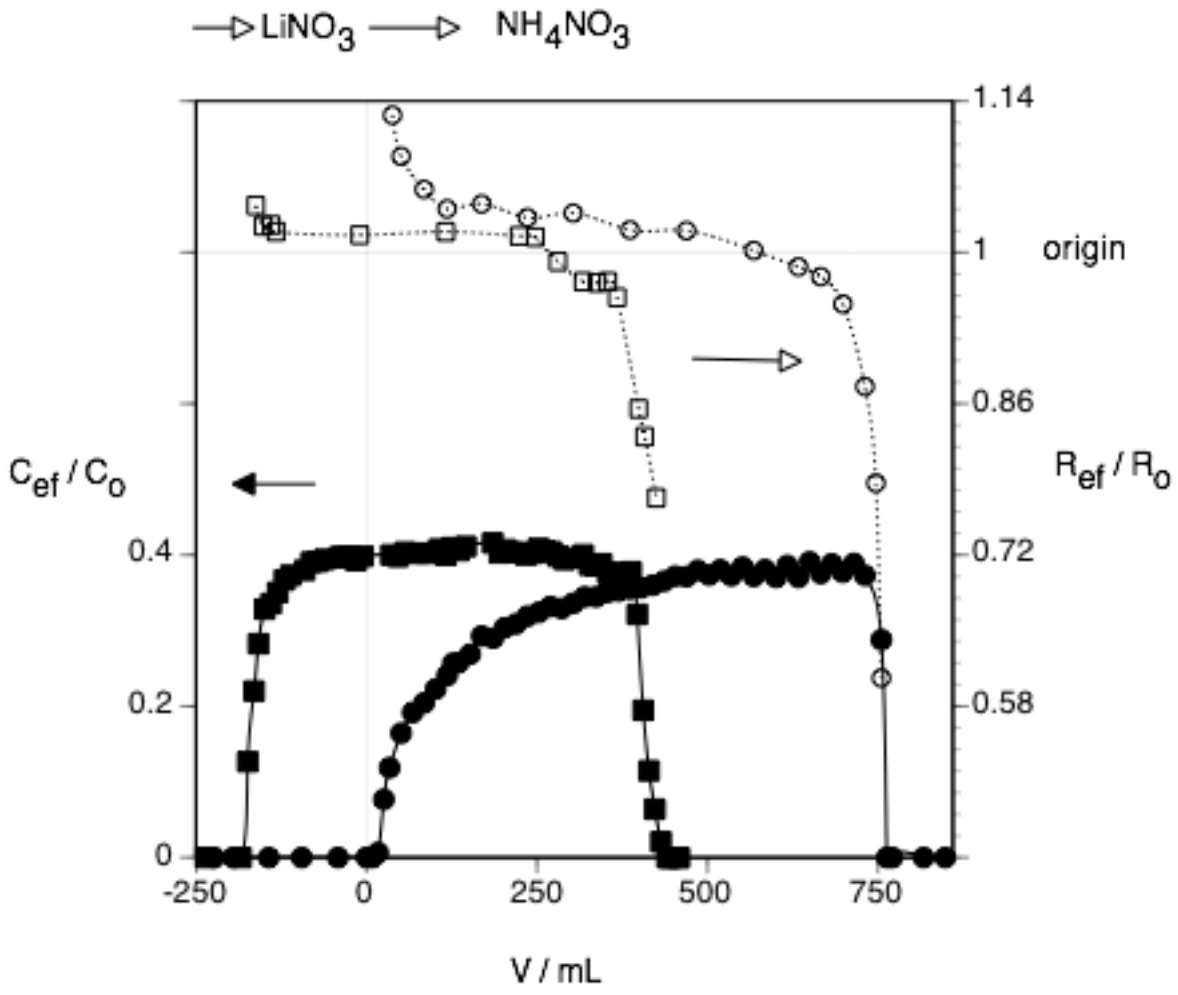

Fig. 2, A. Ishikawa et al

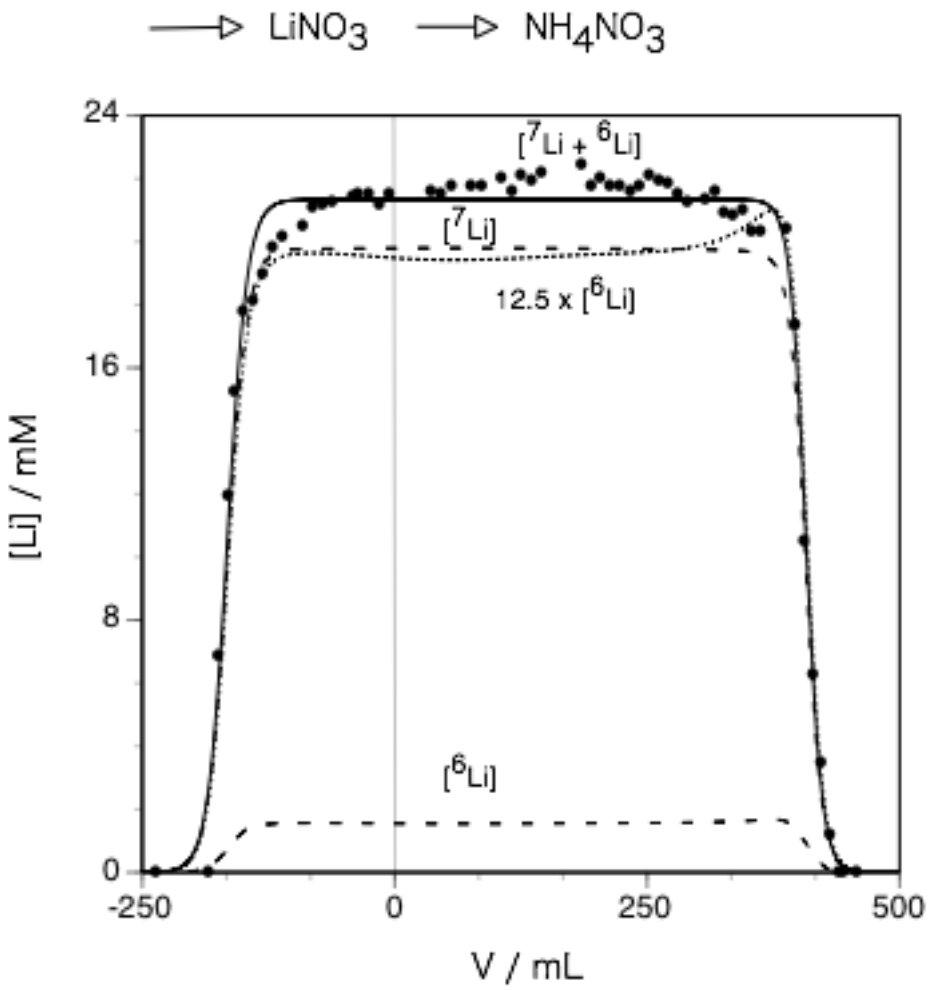

Fig. 3, A. Ishikawa et al.

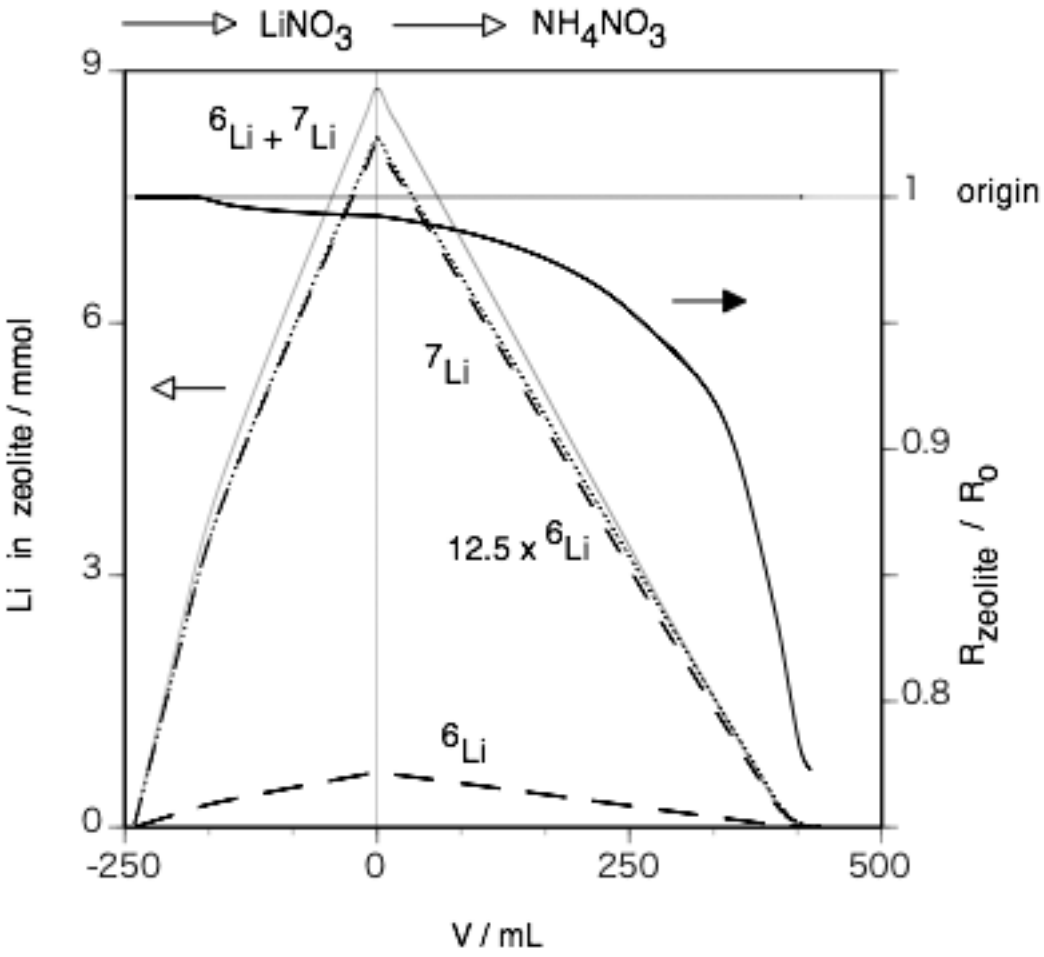

Fig. 4, A. Ishikawa et al.

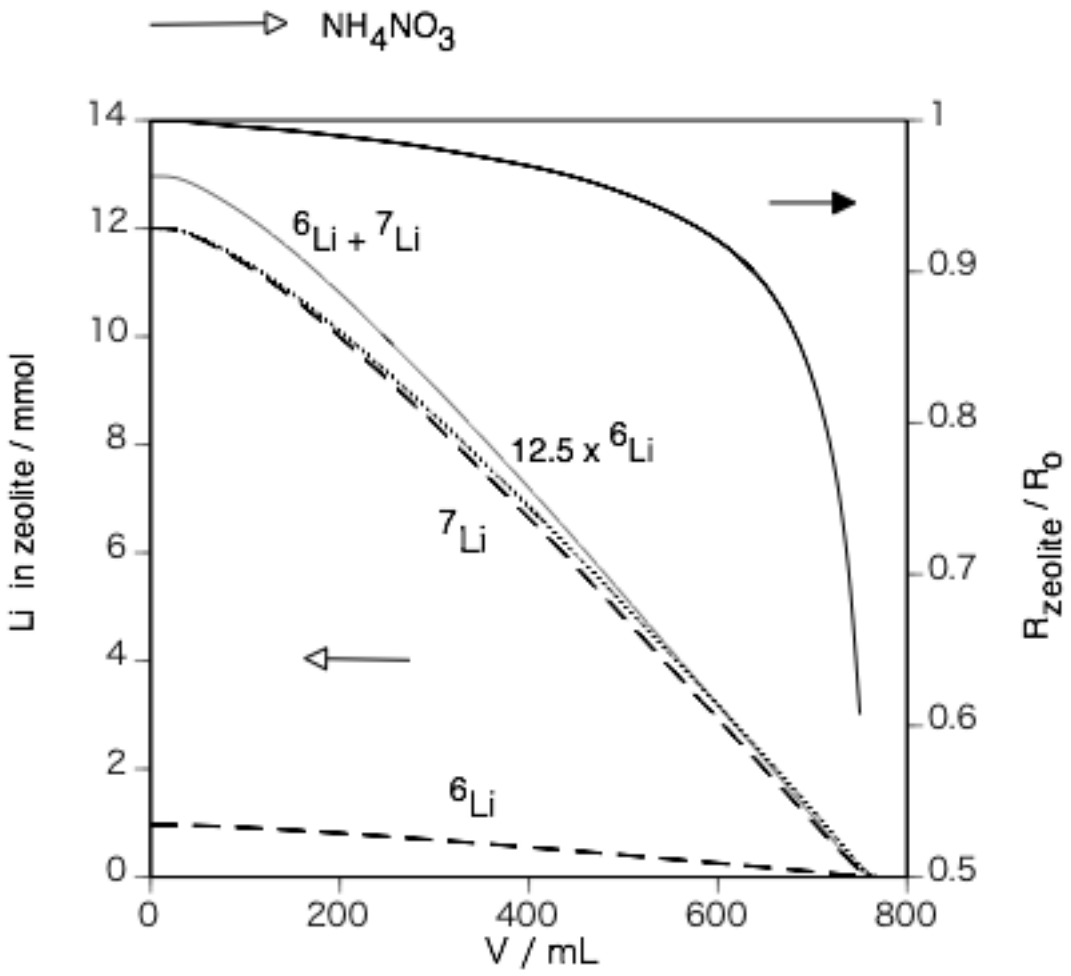

Fig. 5, A. Ishikawa et al.

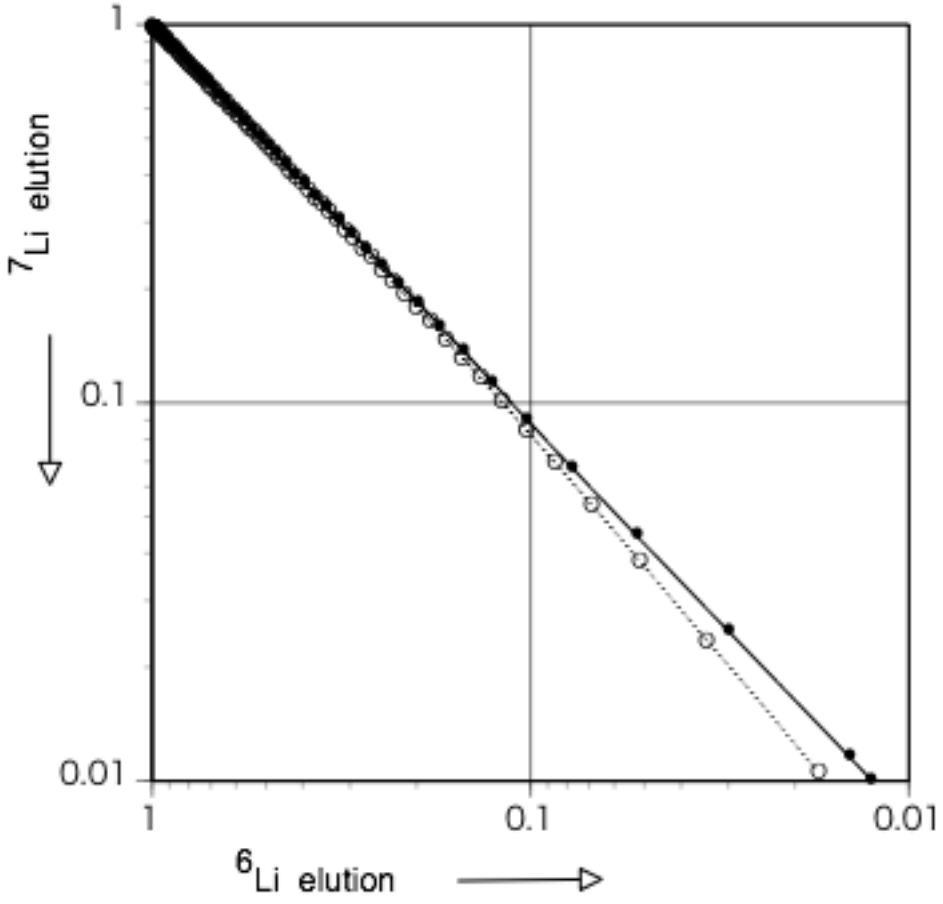

Fig. 6, A. Ishikawa et al.

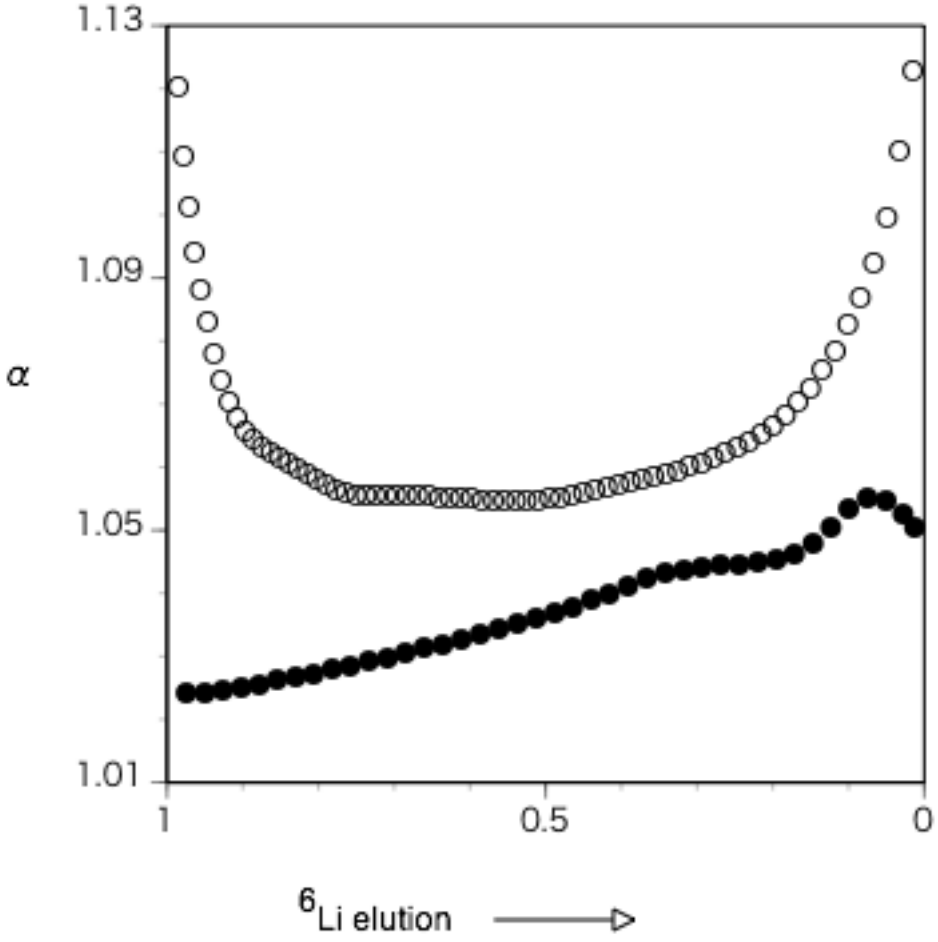

Fig. 7, A. Ishikawa et al.

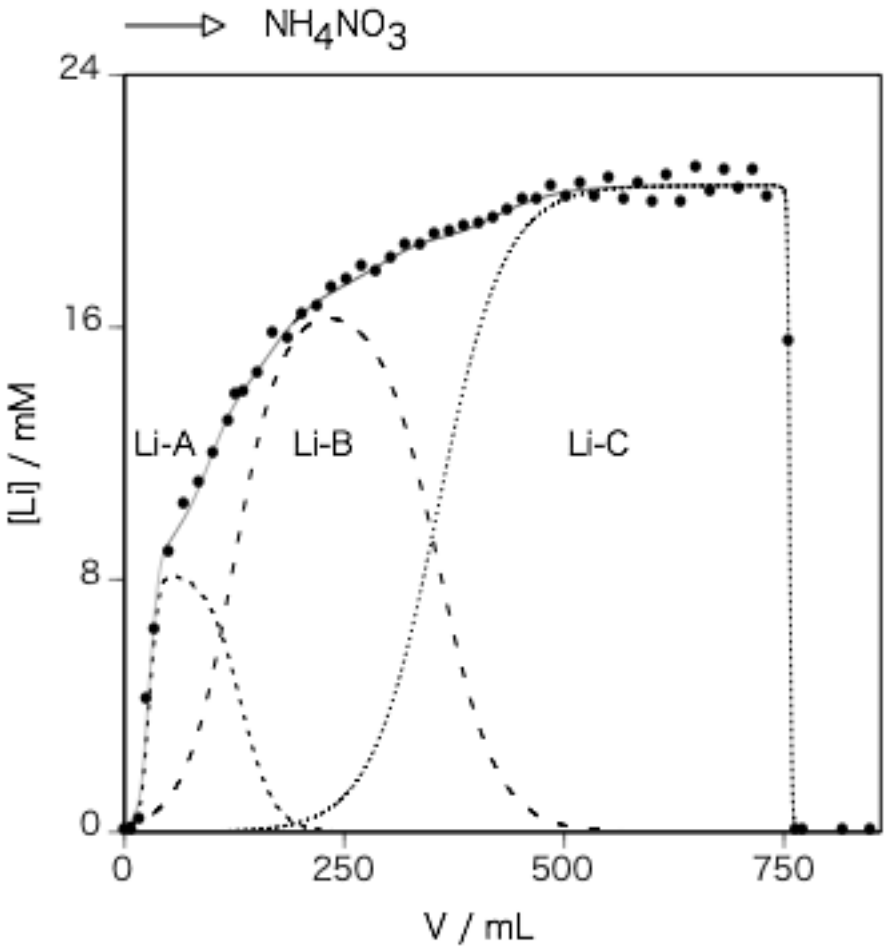

Fig. 8, A. Ishikawa et al.

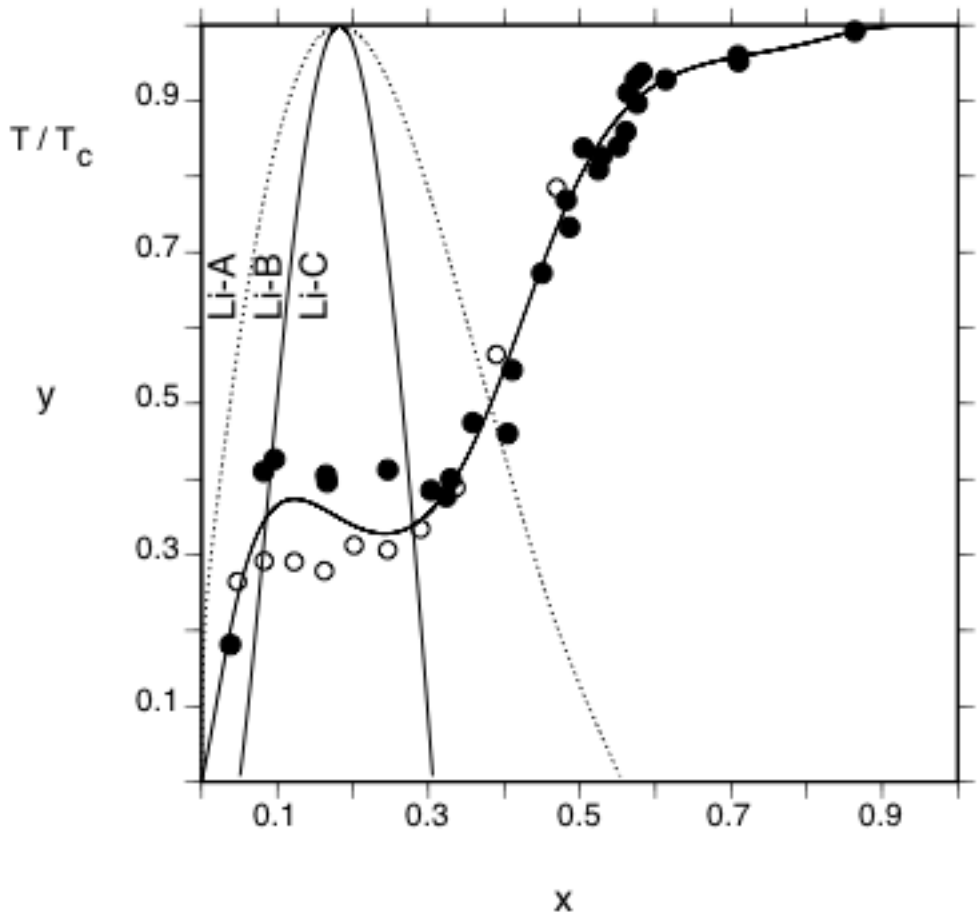

Fig. 9, A. Ishikawa et al.

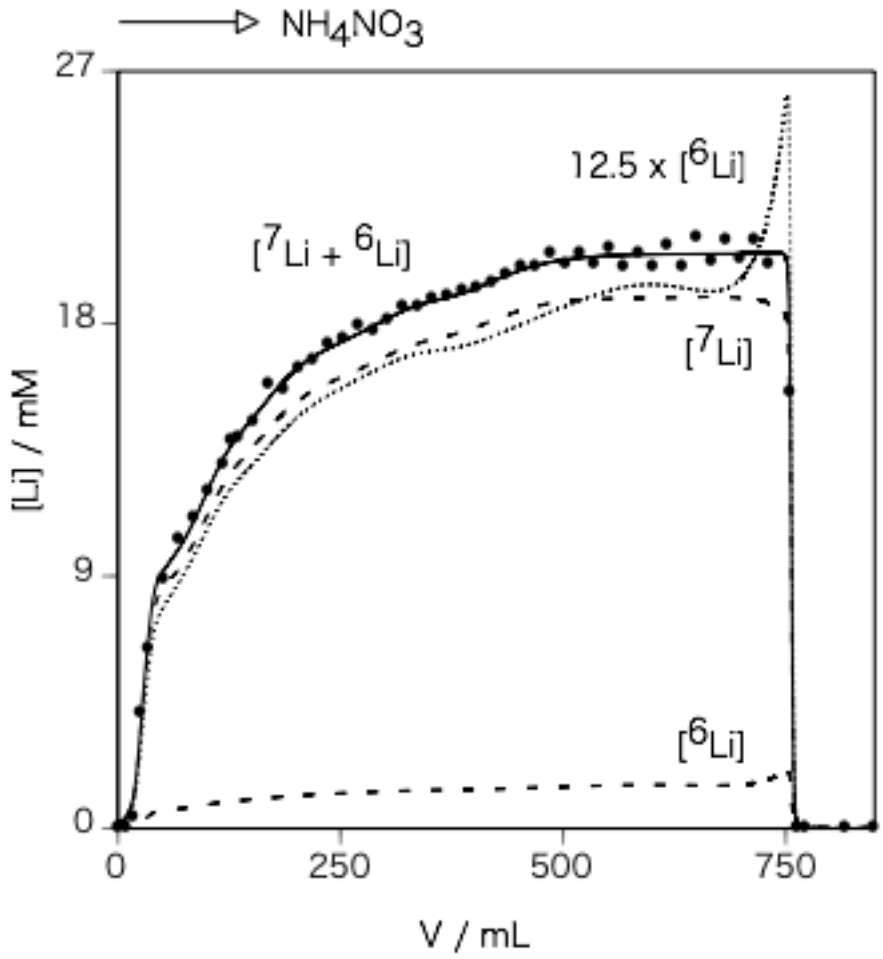

Fig. 10, A. Ishikawa et al.

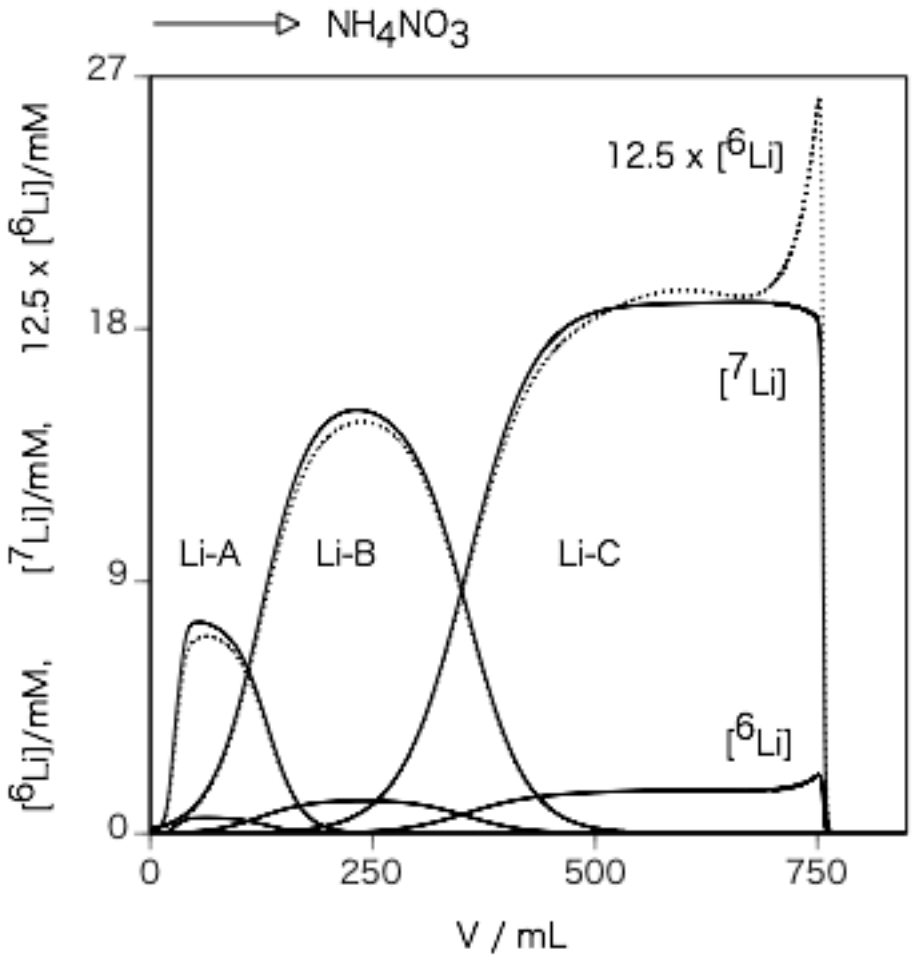

Fig. 11, A. Ishikawa et al.